Available online at www.sciencedirect.com

ScienceDirect

IFAC Papers Online CONFERENCE PAPER ARCHIVE

IFAC PapersOnLine 59-30 (2025) 203–208

Comparative Analysis of Fingertip Location for the SMU Haptic Glove by OptiTrack Cameras and Embedded Position Sensors

Ammar Yacoub, Edmond Richer, Yildirim Hurmuzlu

Southern Methodist University, Dallas, TX 75205 USA

(e-mail: ayacoub@smu.edu, richer@lyle.smu.edu, hurmuzlu@lyle.smu.edu)

Abstract: This paper presents an analysis of the precision of fingertip location for a 7 degrees of freedom (DOF) pneumatic haptic glove developed at SMU for 3D elastographic imaging virtual palpation. The 2D workspace for each finger and the 3D workspace for the glove are calculated from the actuator positions using closed-form expressions based on design geometry. The fingertip locations are measured using a 5-camera OptiTrack motion capture, and the results are compared with the fingertip positions obtained using the linear sensors integrated in the design of each finger joint. This work is an essential step in the development of a virtual palpation system of 3D elastographic medical images.

Keywords: Haptics, Robotic Exoskeleton, Motion Capture, Virtual Palpation.

1. INTRODUCTION

Physicians use their sense of touch to examine and detect abnormalities in tissue, Bickley and Szilagyi (2012), by recognizing differences in their mechanical properties. This diagnostic technique, known as medical palpation, is widely used to help diagnose life-threatening conditions such as cancer, Scimeca et al. (2022). However, palpation is limited to superficial organs and requires extensive experience and training. In recent years, ultrasound and magnetic resonance elastography imaging techniques have become crucial for diagnosing cancerous tumors and liver fibrosis by assessing the mechanical properties of tissue in both shallow and deep organs, Sigrist et al. (2017); Pepin et al. (2015).

Advancements in computer technology, imaging techniques, and nonlinear control algorithms allow the integration between 3D elastographic images and a haptic interface for the hand into a virtual reality haptic system (VRHS). This system creates a unique technological opportunity for opening the entire human body to the medical professionals for virtual palpation of suspected malignant tumors or other abnormal tissue, Palmerius et al. (2011).

Haptic systems have been successfully utilized in virtual reality surgical training, Gani et al. (2022), robot-assisted surgery Enayati et al. (2016), and telemechanics. However, the current haptic interface typically involves a basic stylus or a simple tactile display that limits the haptic palpation of elastographic images, Palmerius et al. (2011). To empower doctors to fully utilize their training and experience in medical palpations, it is essential to have a haptic interface that incorporates multiple interaction points located at their fingertips, such as a haptic glove.

Most haptic gloves, such as the Cyber Grasp by Cyber Glove Systems Glove (2016) and the Dexmo Glove Gu et al. (2016), along with an exoskeleton proposed in Sarakoglou et al. (2016) and Ma and Ben-Tzvi (2015), fail to control all degrees of freedom in the fingers, instead operating on the collective movement of the finger joints. This simple finger-bending model is adequate for approximating the grasp of a virtual object and providing realistic force feedback to the operator. However, multiple fingertip positions may correspond to the exact location of the haptic actuators, and their capacity to render force direction at the fingertip is significantly limited.

Virtual palpation requires an accurate model of the haptic glove to effectively compute the fingertip's location and respond to subtle joint movements, allowing for the rendering of kinesthetic and tactile sensations across multiple locations. The haptic glove developed by the authors accurately determines fingertip positioning using a minimal number of sensors and actuators, all while maintaining user comfort and freedom of movement.

2. HAPTIC GLOVE DESIGN AND KINEMATIC ANALYSIS

The haptic glove shown in Fig. 1 was developed at Lyle School of Engineering at SMU for virtual palpation of 3D elastographic imaging, Galla et al. (2020, 2019). The glove mounts over the back of the hand and interfaces with the distal phalanges of the user's index and middle fingers, and the thumb. These fingers, primarily used during palpation, have a total of 13 degrees of freedom (DOFs). For design simplicity, while maintaining the requirements of palpation, six degrees are actuated and measured, one degree is measured without actuation, and two DOFs are coupled with others using a 1:1 gear mechanism, for a total of 7 DOFs of the Haptic Glove (Table 1). The active joints are driven by pneumatic cylinders, with linear sensors aligned with the cylinders measuring their stroke.

The glove features nine adjustable connections strategically positioned to fit the most important points of the hand: two adjustments for the length of each finger, two adjustments linking the middle and thumb to the palm,

10.1016/j.ifacol.2025.12.237

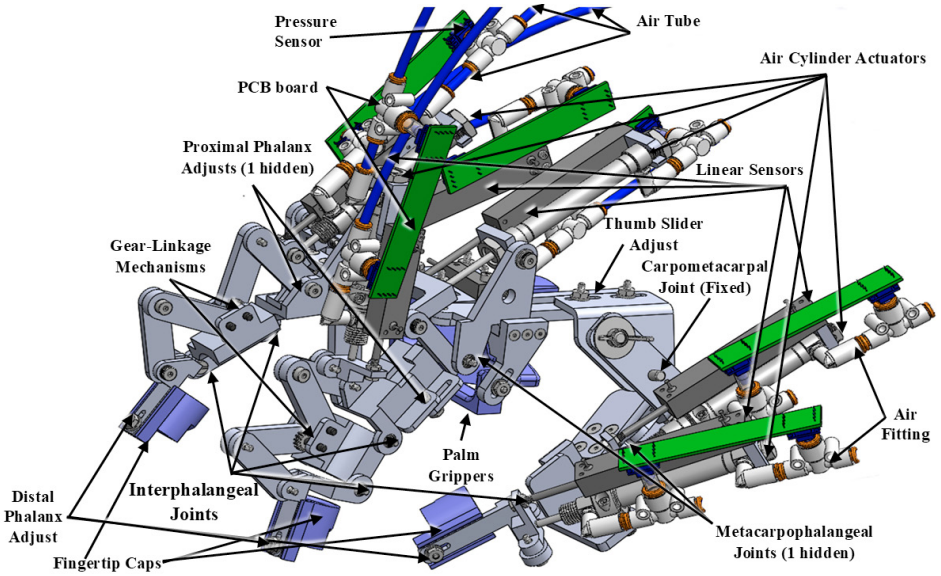

Fig. 1. SMU Haptic Glove CAD representation.

Table 1. Joint Actuation Table for Index and Middle Fingers, and Thumb.

Joint Name	Movement Type	Index Finger	Middle Finger	Thumb
Distal Interphalangeal	Flexion/Extension	Constrained (via gearing mechanism)		—
Proximal Interphalangeal (θ_{j2})	Flexion/Extension	Actuated	Actuated	Actuated
Metacarpophalangeal (θ_{j1})	Flexion/Extension	Actuated	Actuated	Actuated
Metacarpophalangeal (θ_{j3})	Abduction/Adduction	Measured	Fixed	Fixed
Carpometacarpal	Flexion/Extension	—	—	Fixed
Carpometacarpal	Abduction/Adduction	—	—	Fixed

and one regarding palm size. These features ensure compatibility with a wide range of users, as the size and shape of hands vary; even the two hands of a single individual are neither identical nor perfectly symmetrical, Perret and Vander Poorten (2018).

The haptic glove design comprises four main substructures: the index finger, the middle finger, the thumb, and the palm. The following subsection will provide an overview of substructure design and kinematics analysis.

2.1 Substructure Design

The design of the index finger substructure is detailed in Galla et al. (2020), and Richer et al. (2023). Additionally, the middle finger design is very similar to the index finger, with the key difference being that it is longer and that the abduction/adduction motion of the metacarpophalangeal (MCP) joint is fixed. Conversely, the thumb design, shown in Fig. 2, differs from the other fingers due to the absence of a gear mechanism, as it has only one interphalangeal (IP) joint. The MCP and IP flexion/extension motions are actuated by separate pneumatic cylinders, meaning that the two DOFs are uncoupled. The abduction and adduction of the MCP joint, along with both flexion/extension and abduction/adduction of the carpometacarpal joint, are fixed. Finally, a release mechanism enables users to remove the thumb substructure quickly.

The three finger substructures are anchored to the central palm substructure, shown in Fig. 3. The central plate of the palm substructure is secured over the user's hand by three adjustable braces that wrap around the palm. The MCP joint of the index finger allows the abduction/adduction of the index finger up to 20° away from the middle finger, without being actuated.

2.2 Kinematic Analysis

A geometric analytical approach (more detailed in Galla et al. (2020)) was employed for kinematics analysis to determine the transformation functions from actuator positions, measured with linear sensors, to the angles of each joint. In the following equations, the first subscript, $j = 1 - 3$ represents the index, middle finger, and thumb, respectively. The second subscript represents the MCP joint flexion/extension, $k = 1$, the proximal IP

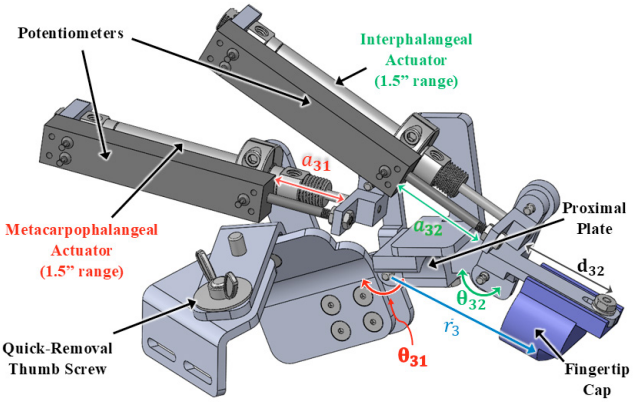

Fig. 2. Thumb design and its actuated degrees of freedom.

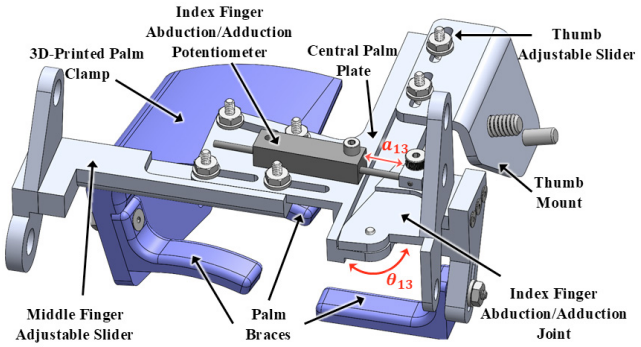

Fig. 3. Palm substructure viewed from the fingertip perspective.

joint flexion/extension, $k = 2$, and MCP joint abduction/adduction, $k = 3$.

The flexion of the MCP joint (θ_{j1}) can be calculated using the displacement of the MCP actuator (a_{j1}) and is defined by Eq. 1. In the same way, the flexion of the IP joint (θ_{j2}) is derived from Eq. 2 and can be calculated using the displacement of the proximal IP joint actuator (a_{j2}).

$$\begin{aligned}\theta_{11} &= \cos^{-1}\left(1.092 - 2.895\times10^{-4}a_{11}^2\right) - 0.207\ \pi,\\ \theta_{21} &= \cos^{-1}\left(1.023 - 3.352\times10^{-4}a_{12}^2\right) - 0.232\ \pi,\\ \theta_{31} &= \cos^{-1}\left(1.107 - 2.996\times10^{-4}a_{31}^2\right) - 0.18\ \pi.\end{aligned} \tag{1}$$

$$\begin{aligned}\theta_{12} &= 2\cos^{-1}\left(\frac{25.38 - 33\cos\theta_{1g}}{\sqrt{1733.06 - 1674.97\cos\theta_{1g}}}\right) - 0.210\ \pi,\\ \theta_{22} &= 2\cos^{-1}\left(\frac{27.415 - 33\cos\theta_{2g}}{\sqrt{1840.56 - 1809.37\cos\theta_{1g}}}\right) - 0.269\ \pi,\\ \theta_{32} &= \cos^{-1}\left(1.058 - 3.036\times10^{-4}a_{32}^2\right) - 0.172\ \pi.\end{aligned} \tag{2}$$

$$\theta_{13} = 0.349066 - \tan^{-1}\left(\frac{8.5 - 2.4a_{13}}{23.35}\right) \tag{3}$$

Where θ_{1g} and θ_{2g} are the angles of the gear mechanism constraining the proximal and distal IP joints.

$$\begin{aligned}\theta_{1g} &= \sin^{-1}\left(1.479 - 6.477\times10^{-4}a_{12}^2\right) + 0.509\ \pi,\\ \theta_{2g} &= \sin^{-1}\left(1.587 - 5.933\times10^{-4}a_{22}^2\right) + \frac{\pi}{2}.\end{aligned} \tag{4}$$

Table 2 summarizes the range of angles for each joint motion.

Table 2. Range of Motion of Finger Joints for Flexion-Extension Movement.

Finger	MCP θ_{j1}[°]	PIP θ_{j2}[°]	DIP θ_{j2}[°]
Index	0-72.0	0-90.0	0-90.0
Middle	0-76.7	0-90.0	0-90.0
Thumb	0-73.1	-	0-69.2

The fingertip location vector $\bar{r}_j = [x_j, y_j]^T$ is defined using the MCP joint angle θ_{j1}, the IP joint angle θ_{j2}, the adjusted length of the proximal phalanx d_{j1}, and the adjusted fingertip length d_{j2}. The following equation defines the fingertip positions for the three fingers:

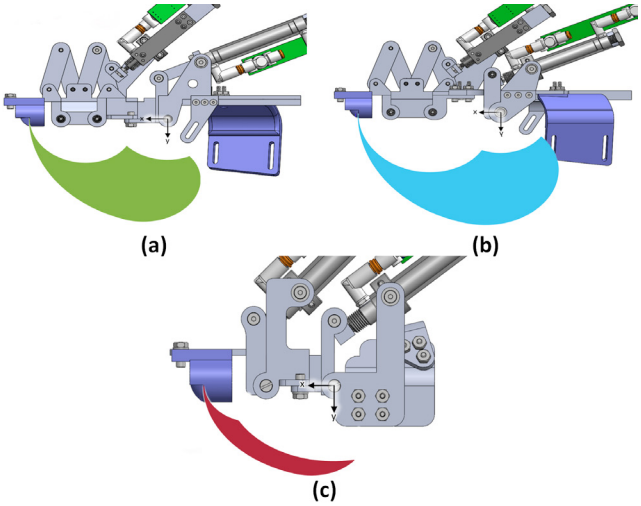

Fig. 4. 2D planar workspace of each finger: (a) Index, (b) Middle, and (c) Thumb.

$$\begin{aligned}\bar{r}_1 &= d_{11}\begin{bmatrix}\cos(\theta_{11})\\ \sin(\theta_{11})\end{bmatrix} + 25\begin{bmatrix}\cos(\theta_{11}+\theta_{12})\\ \sin(\theta_{11}+\theta_{12})\end{bmatrix} + d_{12}\begin{bmatrix}\cos(\theta_{11}+2\theta_{12})\\ \sin(\theta_{11}+2\theta_{12})\end{bmatrix},\\ \bar{r}_2 &= d_{21}\begin{bmatrix}\cos(\theta_{21})\\ \sin(\theta_{21})\end{bmatrix} + 31\begin{bmatrix}\cos(\theta_{21}+\theta_{22})\\ \sin(\theta_{21}+\theta_{22})\end{bmatrix} + d_{22}\begin{bmatrix}\cos(\theta_{21}+2\theta_{22})\\ \sin(\theta_{21}+2\theta_{22})\end{bmatrix},\\ \bar{r}_3 &= d_{31}\begin{bmatrix}\cos(\theta_{31})\\ \sin(\theta_{31})\end{bmatrix} + d_{32}\begin{bmatrix}\cos(\theta_{31}+\theta_{32})\\ \sin(\theta_{31}+\theta_{32})\end{bmatrix}.\end{aligned} \tag{5}$$

Figure 4 shows the workspace of each finger, assuming the origin location at the MCP joint, the x-axis positively oriented toward the fingertip of the outstretched palm, and the y-axis positively oriented in the direction of finger flexion, Richer et al. (2023).

The 3D workspace for the Haptic Glove is constructed by the union of the 2D workspaces of each finger, as mounted on the palm substructure (see Fig. 5). As previously mentioned, the index MCP joint has an abduction/adduction range of motion of 20° away from the middle finger.

3. EXPERIMENTAL SETUP

The accuracy of fingertip location is crucial in virtual palpation for achieving precise haptic feedback; therefore, an experiment was designed to examine the accuracy of tip location, both by internal sensors and a workspace motion tracking optical system. The overall framework for the experiment is illustrated in Figure 6. Fingertip location is calculated using Eq. 5 by measuring the position of each linear pneumatic actuator using linear position

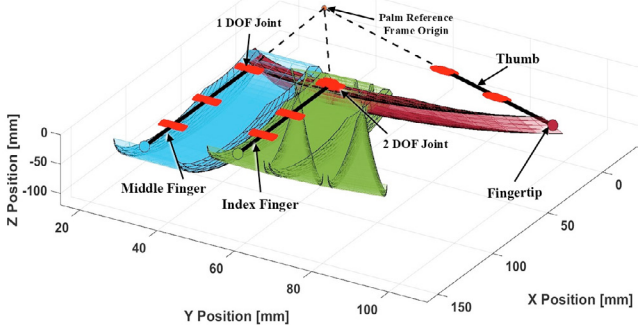

Fig. 5. Three-dimensional workspace of the Haptic Glove.

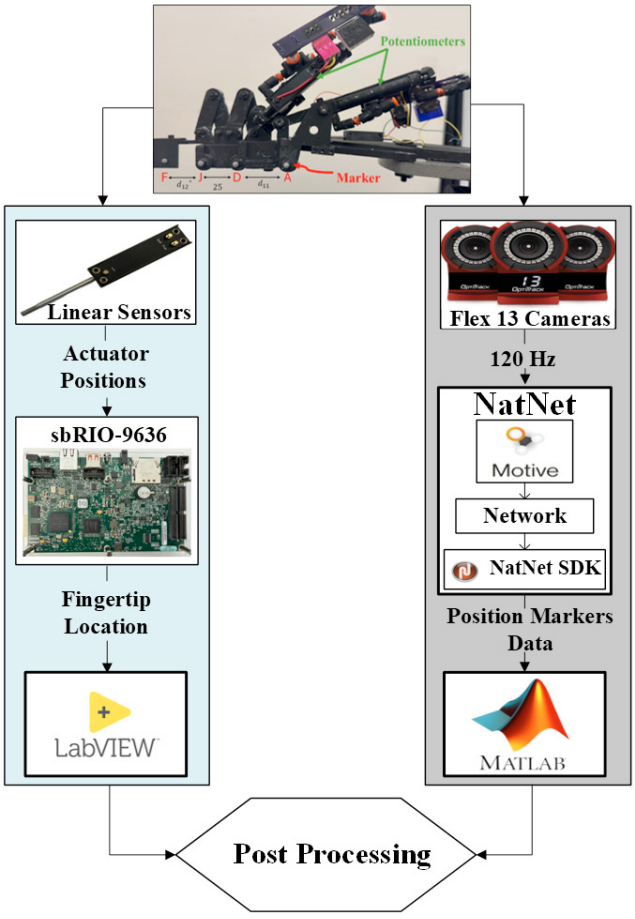

Fig. 6. Framework of the experimental setup.

sensors (potentiometers). The results are compared with the fingertip locations determined using the five OptiTrack cameras, which are considered as the reference.

The experiments were conducted separately for the index finger and thumb: 210 samples were collected from the index finger, while 142 samples were taken for the thumb. Each sample was repeated 10 times to quantify the mechanical, electronic, and optical errors. The results for the middle finger are not presented since it is mechanically identical with the index finger.

A P3 America Series LMC13 linear motion conductive plastic potentiometer is attached alongside each actuator cylinder to measure its stroke. The fingertip location equations are implemented using the LabVIEW programming language on an NI sbRIO-9636 real-time system with an FPGA DAQ module. Each trial's average of 10 consecutive readings at 1 kHz was calculated to account for potential noise from the sensor.

The OptiTrack system, shown in Figure 7, consists of five Flex 13 cameras that capture passive markers and a 3-axis tripod to position the finger substructure accurately. The Flex 13 camera offers a resolution of 1.3 million pixels at a sampling rate of 120 frames per second (FPS), and it works in conjunction with Motive Tracker 2.0 Software. Passive markers with a diameter of 4 mm are affixed to each joint, and an additional marker is placed on a new finger cap design for tracking purposes, as illustrated in Figure 8. A NatNet SDK server version 4.1 is employed to

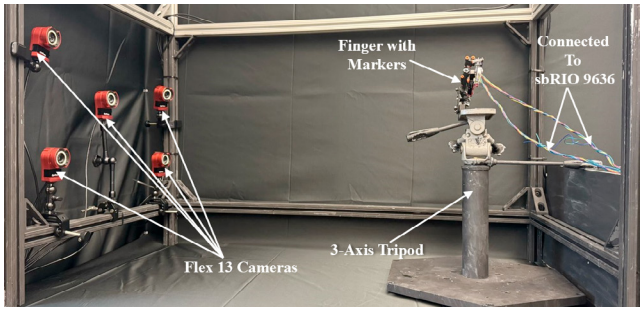

Fig. 7. Experimental setup of OptiTrack motion capture.

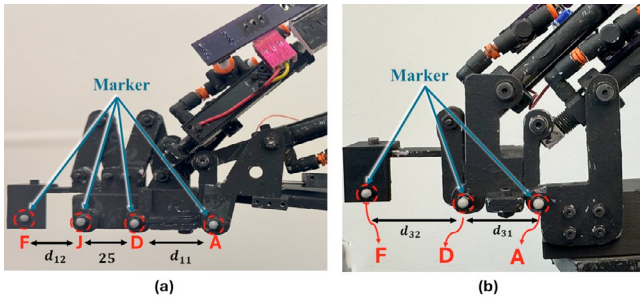

Fig. 8. Finger with passive markers: (a) index finger, (b) thumb.

stream marker position data over a network and interface with MATLAB using a ".NET" interface. The custom MATLAB code reads each marker's position and calculates the fingertip location.

4. RESULT

Each sample measurement was repeated ten times. Figure 9 shows a box plot illustrating the standard deviation of repeated measurements for the x and y positions of the index finger and thumb. The maximum standard deviation values for the index finger's x and y positions are 1.04 mm and 0.70 mm, respectively. For the thumb, the maximum standard deviation values for the x and y positions are 0.36 mm and 0.41 mm, respectively. Additionally, the mean value for the index finger is approximately 0.3 mm for both the x and y positions, while it is 0.27 mm for the x position and 0.17 mm for the y position of the

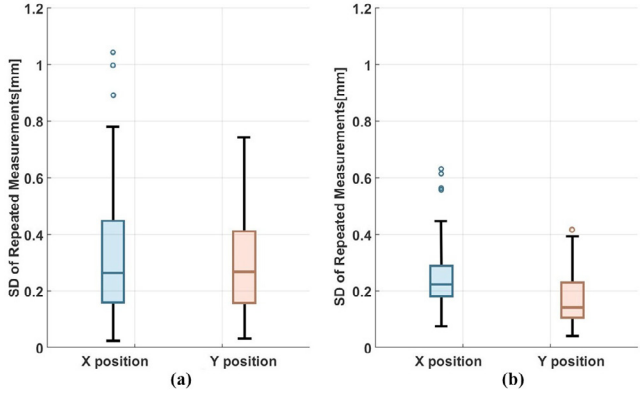

Fig. 9. Box chart of the standard deviation of repeated measurements for each sample comparing OptiTrack cameras data and the embedded sensors reading for fingertip location : (a) index finger, (b) thumb.

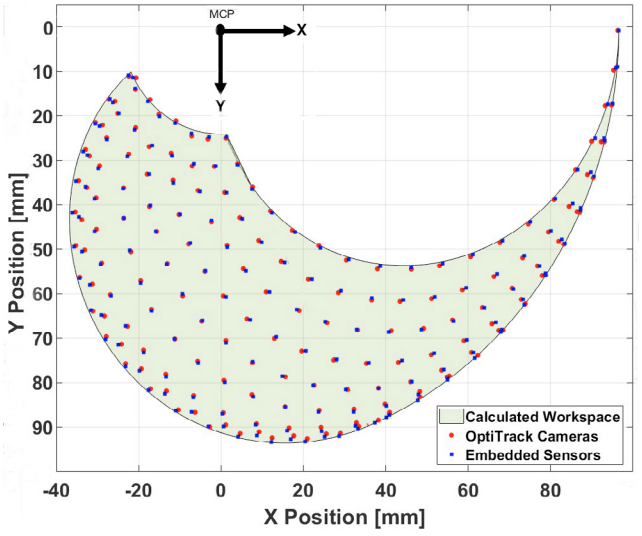

Fig. 10. Comparison of index finger position measurements using OptiTrack cameras and embedded sensors.

thumb. These results indicate high consistency and precise measurement processes.

4.1 Index Finger

Figure 10 shows the distribution of 210 samples of index finger fingertip positions measured with the OptiTrack cameras and calculated using the embedded sensors within the entire workspace. The histogram of the difference between x and y position measurements obtained using the two aforementioned methods is shown in Fig. 11. Potential sources of error include sensor noise, gear backlash, and joint clearance. The maximum absolute differences for the x and y positions are 1.25 mm and 1.00 mm, respectively. The standard deviations and root mean square values for the x and y positions are approximately 0.48 mm and 0.41 mm, respectively. Furthermore, 126 samples (60% of the total) for x position and 154 samples (73% of the total) for y position have an absolute difference of less than 0.5 mm, demonstrating the high precision of the embedded sensors and the accuracy of the index finger substructure construction in determining the location of the fingertip.

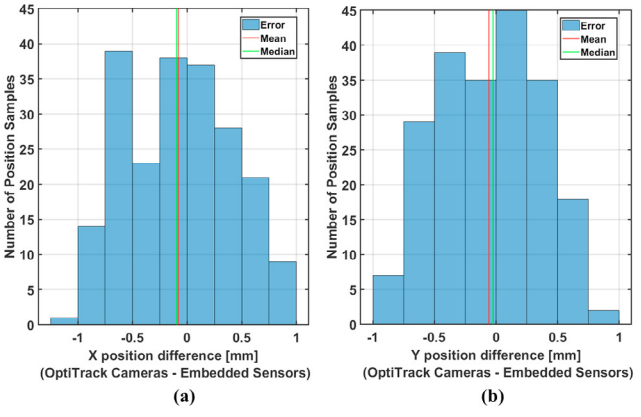

Fig. 11. Distribution of the difference in index finger position between OptiTrack cameras and the potentiometer: (a) x-position, (b) y-position.

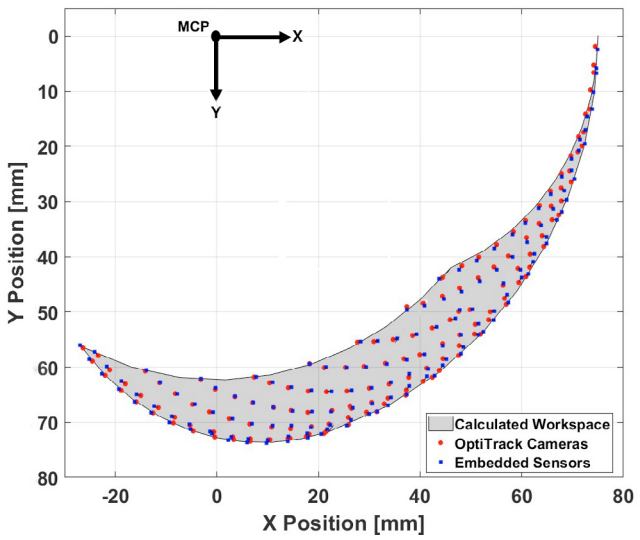

Fig. 12. Comparison of thumb finger position measurements using OptiTrack Cameras and embedded sensors.

4.2 Thumb Finger

The same analysis conducted for the index finger was performed for the thumb. Figure 12 shows 142 samples for the thumb fingertip location. The histogram illustrating the distribution of the differences in x and y position measurements is displayed in Figure 13. The maximum absolute differences for both x and y positions are 1.00 mm, respectively. The root mean square and the standard deviation values for the x and y positions are 0.49 mm and 0.38 mm, respectively. Additionally, 72 samples for the x position (51% of the total), and 106 samples for the y position (75% of the total) have an absolute difference of less than 0.5 mm, reflecting the precision of the thumb substructure design to locate the fingertip location.

The magnitude of the fingertip location vector can be calculated using the Euclidean norm $|\bar{r}| = \sqrt{x^2 + y^2}$. The distribution of the difference in magnitude between the OptiTrack cameras and the potentiometer for the index and thumb fingers is shown in Fig. 14. For the index finger, 162 samples (77% of the total), and 115 samples

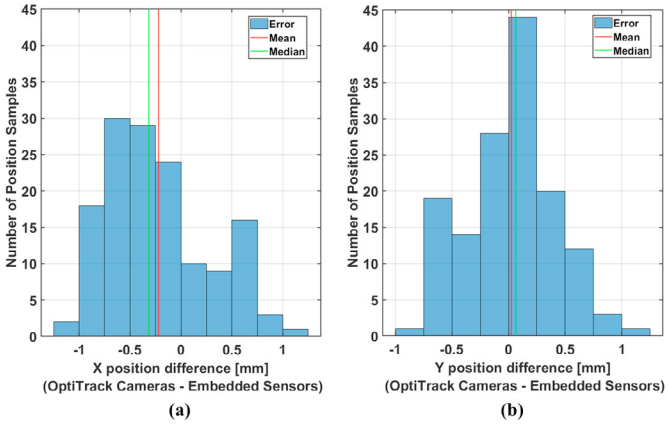

Fig. 13. Distribution of the difference in thumb position between OptiTrack cameras and embedded sensors: (a) x-position, (b) y-position.

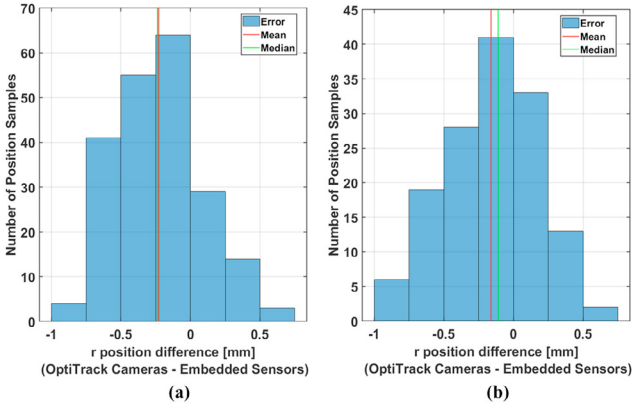

Fig. 14. Distribution of the magnitude of the fingertip location vector $\overline{r}$ difference between OptiTrack cameras and the embedded sensors for (a) index finger and (b) thumb.

(80% of the total) for the thumb have an absolute difference of magnitude of the fingertip location vector less than 0.5 mm. Also, the root mean square for the difference is 0.38 mm and 0.36 mm for the index finger and thumb, respectively. The standard deviation is approximately 0.31 mm for both fingers.

5. CONCLUSION

This paper presents the closed-form equations for fingertip location, the 2D workspace for each fingertip, and the 3D workspace for the assembled Haptic Glove. The location of the fingertips determined using the embedded position sensors was compared with the reference external measurements utilizing a multi-camera optical motion tracking system. The experimental results demonstrate the accuracy of fingertip localization for the index finger and thumb using the embedded sensor system, with an absolute error of less than 1 mm. The mean of the standard deviation is less than 0.3 mm for repeated measurements, indicating high consistency and precise measurements.

Future work on this project will involve examining the precision of grasping and pinching in 3D, as well as developing an accurate dynamic model and implementing a directional force controller for the three fingers. This will be followed by experimental validation using 3D elastographic images in a virtual environment.

ACKNOWLEDGEMENTS

This work was partially supported by NSF Grant 1623324.

REFERENCES

Bickley, L. and Szilagyi, P.G. (2012). *Bates' guide to physical examination and history-taking.* Lippincott Williams & Wilkins.

Enayati, N., De Momi, E., and Ferrigno, G. (2016). Haptics in robot-assisted surgery: Challenges and benefits. *IEEE reviews in biomedical engineering*, 9, 49–65.

Galla, M.E., Al Khatib, E.I., Hurmuzlu, Y., and Richer, E. (2019). Force and stiffness controller design for a pneumatic haptic glove for virtual palpation. In *Dynamic Systems and Control Conference*, volume 59148, V001T05A012. American Society of Mechanical Engineers.

Galla, M.E., Al Khatib, E.I., Richer, E., and Hurmuzlu, Y. (2020). Design and nonlinear control of a haptic glove for virtual palpation. In *2020 American Control Conference (ACC)*, 551–556. IEEE.

Gani, A., Pickering, O., Ellis, C., Sabri, O., and Pucher, P. (2022). Impact of haptic feedback on surgical training outcomes: a randomised controlled trial of haptic versus non-haptic immersive virtual reality training. *Annals of Medicine and Surgery*, 83, 104734.

Glove, C. (2016). Cyberglove systems inc.

Gu, X., Zhang, Y., Sun, W., Bian, Y., Zhou, D., and Kristensson, P.O. (2016). Dexmo: An inexpensive and lightweight mechanical exoskeleton for motion capture and force feedback in vr. In *Proceedings of the 2016 CHI Conference on Human Factors in Computing Systems*, 1991–1995.

Ma, Z. and Ben-Tzvi, P. (2015). Design and optimization of a five-finger haptic glove mechanism. *Journal of Mechanisms and Robotics*, 7(4), 041008.

Palmerius, K.L., Havre, R.F., Gilja, O.H., and Viola, I. (2011). Ultrasound palpation by haptic elastography. In *2011 24th International Symposium on Computer-Based Medical Systems (CBMS)*, 1–6. IEEE.

Pepin, K.M., Ehman, R.L., and McGee, K.P. (2015). Magnetic resonance elastography (mre) in cancer: Technique, analysis, and applications. *Progress in nuclear magnetic resonance spectroscopy*, 90, 32–48.

Perret, J. and Vander Poorten, E. (2018). Touching virtual reality: a review of haptic gloves. In *ACTUATOR 2018; 16th International Conference on New Actuators*, 1–5. VDE.

Richer, E., Galla, M., and Hurmuzlu, Y. (2023). Directional force feedback for a 3 dof pneumatic haptic finger. *IFAC-PapersOnLine*, 56(3), 295–300.

Sarakoglou, I., Brygo, A., Mazzanti, D., Hernandez, N.G., Caldwell, D.G., and Tsagarakis, N.G. (2016). Hexotrac: A highly under-actuated hand exoskeleton for finger tracking and force feedback. In *2016 IEEE/RSJ International Conference on Intelligent Robots and Systems (IROS)*, 1033–1040. IEEE.

Scimeca, L., Hughes, J., Maiolino, P., He, L., Nanayakkara, T., and Iida, F. (2022). Action augmentation of tactile perception for soft-body palpation. *Soft robotics*, 9(2), 280–292.

Sigrist, R.M., Liau, J., El Kaffas, A., Chammas, M.C., and Willmann, J.K. (2017). Ultrasound elastography: review of techniques and clinical applications. *Theranostics*, 7(5), 1303.